

# Clustering with Communication: A Variational Framework for Single Cell Representation Learning

Cong Qi

Yeqing Chen

Jie Zhang

Wei Zhi

New Jersey

New Jersey

Nanjing

New Jersey

Institute of

Institute of

University

Institute of

Technology

Technology

Technology

**Abstract.** Single-cell RNA sequencing (scRNA-seq) has revealed complex cellular heterogeneity, but recent studies emphasize that understanding biological function also requires modeling **cell-cell communication (CCC)**—the signaling interactions mediated by ligand-receptor pairs that coordinate cellular behavior. Tools like CellChat have demonstrated that CCC plays a critical role in processes such as cell differentiation, tissue regeneration, and immune response, and that transcriptomic data inherently encodes rich information about intercellular signaling. We propose **CCCVAE**, a novel variational autoencoder framework that incorporates CCC signals into single-cell representation learning. By leveraging a communication-aware kernel derived from ligand-receptor interactions and a sparse Gaussian process, CCCVAE encodes biologically informed priors into the latent space. Unlike conventional VAEs that treat each cell independently, CCCVAE encourages latent embeddings to reflect both transcriptional similarity and intercellular signaling context. Empirical results across four scRNA-seq datasets show that CCCVAE improves clustering performance, achieving higher evaluation scores than standard VAE baselines. This work demonstrates the value of embedding biological priors into deep generative models for unsupervised single-cell analysis.

## 1. Introduction

A fundamental goal in single-cell transcriptomics is to uncover meaningful biological structures—such as cell types, states, and transitions—by learning informative low-dimensional representations of high-dimensional gene expression data. Among the various computational approaches developed for this task, **Variational Autoencoders (VAEs)** have emerged as a powerful class of generative models that provide a principled probabilistic framework for encoding noisy, sparse, and high-dimensional single-cell RNA sequencing (scRNA-seq) data into compact latent spaces. Models such as *scVI* [Lopez et al., 2018] exemplify how VAEs can capture global patterns in transcriptomic variation and facilitate downstream tasks like imputation, clustering, and differential expression analysis. Despite their success, conventional VAEs treat each cell as an independent observation, focusing primarily on intra-cellular transcriptomic variation. Consequently, the latent representations learned by such models often

fail to reflect key **intercellular biological relationships**—particularly the complex signaling interactions that coordinate cell states in tissues. This limitation becomes especially pronounced in tasks that require biologically structured latent spaces, such as robust clustering or interpretation of cell-cell interactions.

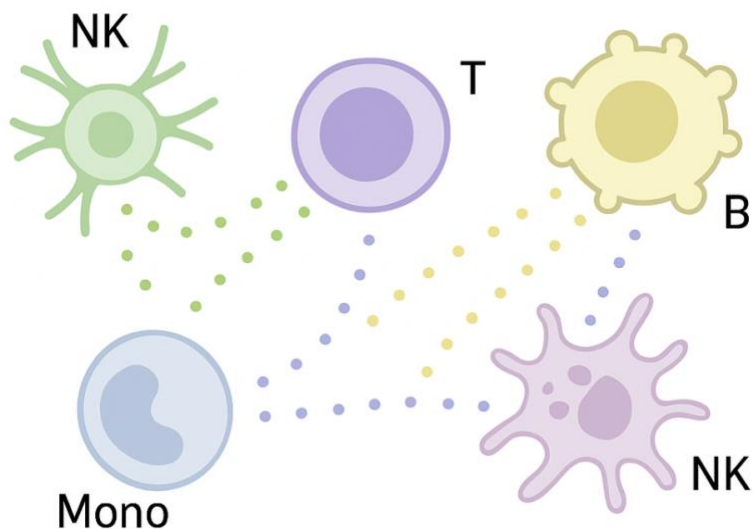


**Figure 1: Schematic representation of intercellular communication among major PBMC subtypes.** Each labeled cell type—NK cells, T cells, B cells, and monocytes—interacts through ligand-receptor signaling, illustrated as colored dots. Ligands secreted by one cell bind to receptors on another, enabling immune coordination. Quantifying the expression levels of ligand-receptor pairs facilitates the study of immune cell communication dynamics in peripheral blood.

One particularly important but underutilized source of biological structure is **Cell-Cell Communication (CCC)**. CCC refers to the biochemical signaling events between cells mediated by ligands, receptors, and cofactors. These signaling pathways regulate processes such as cell differentiation, immune responses, tissue organization, and disease progression. Figure 1 illustrates the CCC mechanism. Recent computational tools—such as *CellChat* [Jin et al., 2021] and *NicheNet*—have demonstrated that CCC can be inferred from scRNA-seq data and used to build detailed intercellular signaling networks. These advances have revealed that CCC is not a peripheral signal but a **driving force behind many biologically meaningful distinctions between cells**.

Motivated by these findings, we propose a new principle for representation learning: *cells that communicate extensively are more likely to belong to different functional clusters, while cells with minimal communication tend to lie within the same cluster*. This insight is biologically grounded—for example, immune cells often signal to epithelial or stromal cells but not among themselves, while cells within a homogeneous lineage (e.g., stem cell niche) communicate

minimally but are transcriptionally similar. To operationalize this idea, we present **CCCVAE**, a novel variational autoencoder that integrates CCC into the latent space via a **communication-aware prior**. Unlike standard VAE-based models that assume an isotropic Gaussian prior for all cells, CCCVAE decomposes the latent representation into two components:

- A **sparse Gaussian Process (GP) prior**, whose kernel is derived from a CCC graph based on ligand-receptor interactions, encodes the communication-informed structure across cells.
- A **standard Gaussian prior**, which captures cell-specific variation not explained by CCC.

During training, the CCC kernel modulates the posterior distribution in the latent space, encouraging cells with higher predicted CCC to be separated in the latent space, while cells with lower communication remain close. This dual-prior design allows CCCVAE to combine biological priors with unsupervised learning in a principled way. Our contributions can be summarized as follows:

- **We propose CCCVAE, the first generative model to incorporate cell-cell communication into single-cell representation learning.** By leveraging a communication-aware Gaussian Process kernel, we directly encode biologically relevant intercellular structure into the latent space.
- **We demonstrate that the learned representations yield significantly better clustering performance** on several benchmark scRNA-seq datasets, including Opium, Pancreas, PBMC4K, and PBMC12K. CCCVAE consistently outperforms baseline methods, including scVI, in Adjusted Rand Index (ARI) and silhouette score.
- **We show that the learned latent space preserves and reflects the underlying CCC structure.** Cells grouped into the same cluster not only share transcriptional similarity but also exhibit low predicted signaling activity with each other, in line with biological expectations.

## 2. Related Work

### Variational Autoencoders for Single-Cell Transcriptomics

Unsupervised representation learning has become essential in decoding the complexity of single-cell RNA sequencing (scRNA-seq) data. Among various approaches, Variational Autoencoders (VAEs) [Kingma and Welling, 2014] offer a generative framework that is both flexible and probabilistic, enabling the modeling of noisy, high-dimensional count data. In the single-cell setting, the generative process typically assumes that each cell  $x_n$  arises from a low-dimensional latent variable  $z_n$  via:

$$z_n \sim \mathcal{N}(0, I), x_n \sim p_\theta(x_n | z_n), \text{ with } p_\theta(x_n | z_n) = \prod_{g=1}^G \text{NB}(x_{ng} | \mu_{ng}(z_n), \theta_g)$$

Here, each gene expression count  $x_{ng}$  is modeled using a Negative Binomial distribution with genespecific dispersion  $\theta_g$ , and the mean  $\mu_{ng}$  is parameterized by a neural decoder  $f_\theta(z_n)$ . The model is trained by maximizing the Evidence Lower Bound (ELBO), which approximates the intractable marginal likelihood:

$$\mathcal{L}_{\text{ELBO}} = \mathbb{E}_{q_\phi(z_n | x_n)}[\log p_\theta(x_n | z_n)] - \text{KL}(q_\phi(z_n | x_n) \parallel p(z_n))$$

This objective balances two competing terms: the reconstruction likelihood of observed data under the generative model, and the Kullback-Leibler divergence between the approximate posterior and the standard normal prior over the latent space. Extensions of this framework, such as scVAE [Grønbech et al., 2020], LDVAE [Gayoso et al., 2020], DCA [Eraslan et al., 2019], and scGen [Lotfollahi et al., 2019], have explored modifications to the decoder architecture or latent prior to improve interpretability and capture dynamic cellular processes. Notably, scVI [Lopez et al., 2018] introduced a hierarchical Bayesian model tailored to scRNA-seq, incorporating additional latent variables for sequencing depth and using variational inference to model gene expression with negative binomial likelihoods.

Despite these advances, most VAE-based models assume that cells are conditionally independent given latent variables, ignoring biologically meaningful dependencies such as intercellular communication or spatial relationships.

### Computational Modeling of Cell-Cell Communication

Cell-cell communication (CCC), mediated by ligand-receptor interactions, plays a vital role in shaping cell fate, function, and tissue structure. Recent tools such as CellChat [Jin et al., 2021], CellPhoneDB [Efremova et al., 2020], and NicheNet [Browaeys et al., 2020] have demonstrated how CCC can be inferred from scRNA-seq data by leveraging curated ligand-receptor interaction databases. These methods typically evaluate the potential communication between cell groups by scoring co-expression of ligand-receptor pairs, either statistically or with regulatory priors, and have uncovered key signaling mechanisms in development, immunity, and cancer.

However, these CCC inference tools are applied in a post hoc manner, detached from the representation learning stage. As a result, learned latent representations from VAEs do not reflect communication-driven dependencies among cells. Although a few models have attempted to incorporate spatial or relational information through graph-based encodings (e.g., spatial-VAE or contrastive approaches), they generally lack a biologically grounded kernel for intercellular communication.

To bridge this gap, we propose CCCVAE, which directly incorporates CCC into the generative modeling process. Specifically, we introduce a communication-aware Gaussian Process prior

over the latent space, with its kernel constructed from a biologically informed ligand-receptor communication matrix. This allows cells with strong signaling relationships to be embedded further apart in the latent space, promoting communication-sensitive clustering while retaining generative interpretability.

### 3. Method

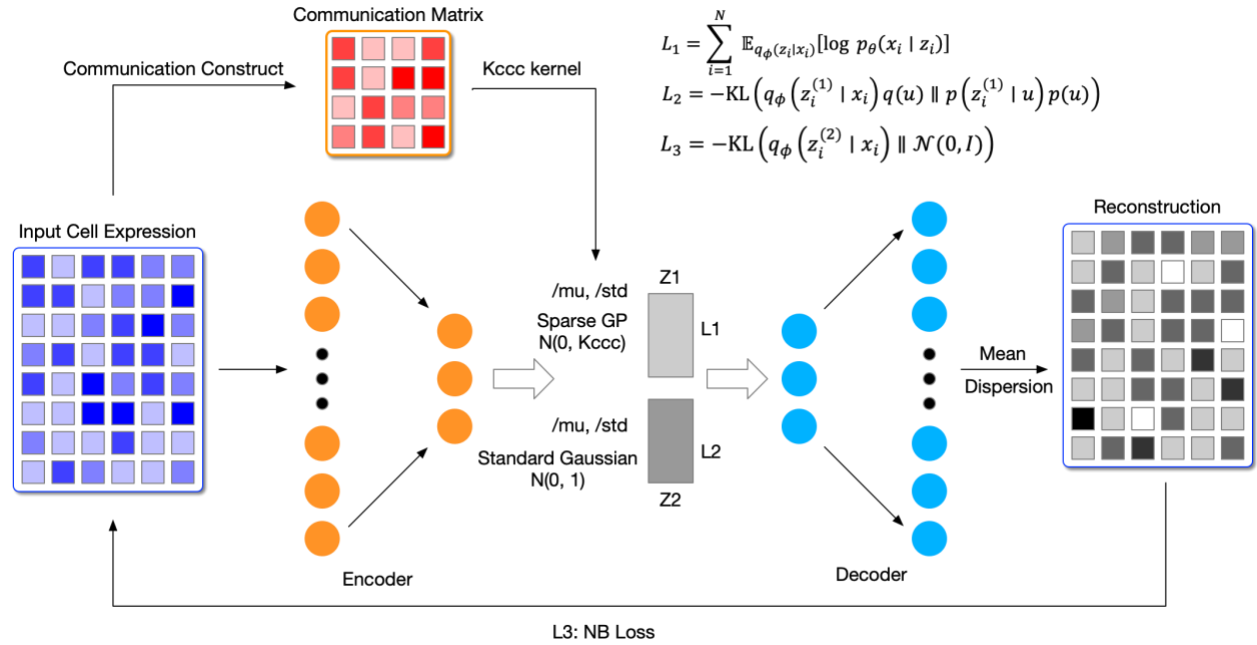


**Figure 2 | The Framework of CCCVAE.** Our CCCVAE framework integrates Cell-Cell Communication (CCC) into a Variational Autoencoder (VAE) via a CCC-informed Gaussian Process. 1. Input: Single-cell gene expression matrix. 2. Communication Matrix: Using CellChat algorithms, we compute a ligand-receptor interaction-based communication matrix (size  $n\_cells \times n\_cells$ ), from which we derive the CCC kernel  $K_{CCC}$ . 3. Encoder: A neural network encodes each cell's expression into latent variables  $\mu$  and  $\sigma$ . 4. CCC-aware Latent Dimensions: The first  $l$  dimensions of  $\mu$  and  $\sigma$  are modeled by a sparse Gaussian Process with kernel  $K_{CCC}$ , encoding inter-cell communication. 5. Remaining Latent Dimensions: The remaining  $D - l$  dimensions are modeled as standard Gaussian variables to capture non-CCC variation. 6. Latent Representation: Latent vectors are sampled from the concatenated distributions. 7. Decoder: A neural network decodes latent vectors back to the gene expression space, predicting mean and dispersion parameters. We use a Negative Binomial loss to handle the overdispersion and sparsity in scRNA-seq data.

We aim to learn low-dimensional representations of single-cell gene expression data that not only preserve biological structure but also reflect meaningful cell-cell communication (CCC) patterns.

To this end, we propose CCCVAE, a novel variational autoencoder that introduces a CCC-aware Gaussian Process (GP) prior over a subset of the latent dimensions. This approach enables a balance between biologically meaningful communication patterns and flexible latent modeling. Figure 2 shows the framework of our CCCVAE model.

### 3.1 VAE Framework for Single-Cell Data

Let  $X = [x_1, \dots, x_N] \in \mathbb{R}^{N \times G}$  denote the gene expression matrix for  $N$  cells and  $G$  genes. In CCCVAE, we learn latent representations  $z_i \in \mathbb{R}^D$  for each cell  $i$ , where  $D$  is the total latent dimensionality.

We partition the latent space as:

$$z_i = \begin{bmatrix} z_i^{(1)} \\ z_i^{(2)} \end{bmatrix}, z_i^{(1)} \in \mathbb{R}^\ell, z_i^{(2)} \in \mathbb{R}^{D-\ell}$$

where:

- $z_i^{(1)}$  (the first  $\ell$  dimensions) encode communication-driven structure governed by a CCC-aware GP prior,
- $z_i^{(2)}$  (the remaining  $D - \ell$  dimensions) model unconstrained variation using a standard Gaussian prior.

This separation allows CCC-relevant information to be structured while maintaining flexibility in modeling residual biological variation.

### 3.2 Constructing the CCC Kernel

The construction of the Cell-Cell Communication (CCC) kernel is central to our model. It incorporates biological communication between cells and ensures positive-definiteness for the Gaussian Process. The kernel construction follows these steps:

#### Step 1: Calculating the Communication Matrix

We start by calculating the communication probability between ligand-receptor pairs, leveraging a detailed formula from the CellChat framework (Jin et al., 2021). This formula models the interaction strength between cells based on gene expression data. For a given ligand  $L_i$  in cell  $i$  and receptor  $R_j$  in cell  $j$ , the communication probability  $P_{ij}$  is calculated as:

$$P_{ij} = \frac{L_i \cdot R_j}{K_h + L_i \cdot R_j} \cdot \left(1 + \frac{AG_i}{K_h + AG_i}\right) \cdot \left(1 + \frac{AG_j}{K_h + AG_j}\right) \cdot \frac{K_h}{K_h + AN_i} \cdot \frac{K_h}{K_h + AN_j} \cdot \frac{(1 + RA_j)}{(1 + RI_j)}$$

Here:

- $L_i$  and  $R_j$  are the expression levels of ligand  $L$  and receptor  $R$  for cells  $i$  and  $j$ , respectively.
- $AG_i, AG_j$  represent the soluble agonists for cells  $i$  and  $j$ , respectively.
- $AN_i, AN_j$  represent antagonists for cells  $i$  and  $j$ .
- $RA_j, RI_j$  represent stimulatory and inhibitory receptors in cell  $j$ .
- $K_h$  is a constant (typically set to 0.5) for normalization.

This equation ensures that the ligand-receptor interaction is modulated by multiple cofactors, including agonists, antagonists, and receptor activities. The geometric mean is used to combine the expressions of multi-subunit ligands and receptors.

## Step 2: Incorporating the Communication Matrix into the Kernel Function

The **Cauchy kernel** is used as the base kernel function, which computes the similarity between cells based on their gene expression. The Cauchy kernel is defined as:

$$K_{\text{Cauchy}}(x_i, x_j) = \frac{1}{1 + \frac{d(x_i, x_j)}{s}}$$

Where:

- $d(x_i, x_j)$  is the squared distance between the feature vectors  $x_i$  and  $x_j$  of cells  $i$  and  $j$ , respectively, and is computed as:

$$d(x_i, x_j) = \|x_i\|^2 + \|x_j\|^2 - 2 \cdot \langle x_i, x_j \rangle$$

where  $\|x_i\|^2$  and  $\|x_j\|^2$  are the squared norms of the gene expression vectors, and  $\langle x_i, x_j \rangle$  is their dot product.

- $s$  is the scale parameter, which controls the width of the kernel and can either be fixed or learnable.

The **communication matrix**  $C_{\text{test, induce}}$  is then integrated into the kernel by applying a **propagation matrix**  $P$  that reflects the cell-cell communication. The propagation matrix is defined as:

$$P = I + \beta \cdot C_{\text{test, induce}}$$

Where:

- $I$  is the identity matrix.

- $\beta$  is a hyperparameter controlling the strength of the communication effect.

The final kernel function, incorporating both the Cauchy kernel and the communication information, is then computed as:

$$K_{\text{CCC}} = K_{\text{Cauchy}} \cdot P \cdot K_{\text{Cauchy}}^T$$

This kernel captures the similarity between test and inducing cells while integrating the cell-cell communication information through the propagation matrix  $P$ . We place the detailed positive-definite property of  $K_{\text{CCC}}$  in appendix A.

### 3.3 Sparse GP Prior for CCC Dimensions

We place an independent sparse variational Gaussian Process prior over each CCC-aware latent dimension  $z_i^{(1)}$ . Given inducing points  $Z_u \in \mathbb{R}^{m \times G}$  and corresponding inducing outputs  $u \in \mathbb{R}^{m \times \ell}$ , the approximate posterior for each dimension  $l$  is:

$$q(f_l(x_i)) = \mathcal{N}(\mu_l(x_i), \sigma_l^2(x_i))$$

where:

$$\begin{aligned} \mu_l(x_i) &= \frac{N}{b} K_{x_i m} \left( K_{mm} + \frac{N}{b} K_{mn} \text{diag}(\sigma^{-2}) K_{nm} \right)^{-1} K_{mn} \text{diag}(\sigma^{-2}) y \\ \sigma_l^2(x_i) &= K_{x_i x_i} - K_{x_i m} K_{mm}^{-1} K_{m x_i} + K_{x_i m} \left( K_{mm} + \frac{N}{b} K_{mn} \text{diag}(\sigma^{-2}) K_{nm} \right)^{-1} K_{m x_i} \end{aligned}$$

Each CCC latent dimension maintains variational parameters  $(\mu_l, A_l)$  approximating  $q(u_l) = \mathcal{N}(\mu_l, A_l)$ . Across all CCC dimensions:

$$p(Z^{(1)} | U^{(1)}) = \prod_{l=1}^{\ell} p(z_{:,l}^{(1)} | u_l)$$

We place the detailed sparse GP prior demonstration in the Appendix B.

### 3.4 Standard Gaussian Prior for Independent Dimensions

For the independent latent variables  $z_i^{(2)}$ , we place a standard isotropic Gaussian prior:

$$p(z_i^{(2)}) = \mathcal{N}(0, I)$$

The variational posterior for  $z_i^{(2)}$  is parameterized by the encoder network as:

$$q_{\phi}(z_i^{(2)} | x_i) = \mathcal{N}\left(\mu_i^{(2)}, \text{diag}\left((\sigma_i^{(2)})^2\right)\right)$$



This structure follows the standard VAE formulation.

### 3.5 Variational Inference and Objective

The overall variational approximation factorizes as:

$$q_\phi(z_i | x_i) = q_\phi(z_i^{(1)} | x_i) q_\phi(z_i^{(2)} | x_i)$$

and the posterior over the inducing variables:

$$q(u) = \mathcal{N}(\mu_u, \Sigma_u)$$

The Evidence Lower Bound (ELBO) for CCCVAE is:

$$\begin{aligned} \mathcal{L}_{\text{CCCVAE}} = & \sum_{i=1}^N \mathbb{E}_{q_\phi(z_i | x_i)} [\log p_\theta(x_i | z_i)] - \text{KL} \left( q_\phi(z_i^{(1)} | x_i) q(u) \parallel p(z_i^{(1)} | u) p(u) \right) \\ & - \text{KL} \left( q_\phi(z_i^{(2)} | x_i) \parallel \mathcal{N}(0, I) \right) \end{aligned}$$

This objective balances:

- Accurate reconstruction of count data via a Negative Binomial likelihood,
- Regularization of CCC-aware latent dimensions via the GP prior,
- Flexibility of unconstrained dimensions to capture residual variability.

## 4. Experiments

### 4.1 Datasets and Baselines

We evaluate our methods on four publicly available single-cell datasets commonly used for benchmarking cell clustering and representation learning:

- PBMC4K: Peripheral blood mononuclear cells (PBMCs) dataset consisting of approximately 4,000 cells.
- Opium: Single-cell RNA-seq dataset profiling human bone marrow treated with opium.
- Pancreas: A pancreas cell dataset collected from multiple donors, exhibiting strong batch effects and cell type diversity.
- PBMC12K: A larger PBMC dataset containing around 12,000 cells, providing a testbed for scalability.

### 4.2 Baseline Methods

We compare our proposed method against the following baseline models:

- Vanilla VAE: A standard Variational Autoencoder with isotropic Gaussian prior and simple reconstruction loss.
- Gaussian Mixture VAE (GMVAE): A VAE variant with a Gaussian Mixture prior to better model clustering structures.
- scVI: A state-of-the-art deep generative model specifically designed for single-cell data, incorporating a Negative Binomial reconstruction loss and batch effect correction.
- CCCVAE: Our proposed model, which integrates Cell-Cell Communication (CCC) information into the latent space via a sparse Gaussian Process prior.

## 4.2 Experimental Setup

For all methods, we use the same encoder and decoder architecture to ensure fair comparison. Training is conducted using the Adam optimizer with an initial learning rate of  $1e^{-3}$  and weight decay of  $1e^{-6}$ . A batch size of 128 is used. The model is trained for a maximum of 50 iterations with early stopping based on a patience of 200 epochs. A KL warmup schedule is applied with  $\beta$  initialized at 0.1 and gradually increased to a maximum of 0.2. For reconstruction loss, we use the Negative Binomial (NB) loss unless otherwise specified. All experiments are repeated with three random seeds, and average results are reported. The primary evaluation metrics are:

- Adjusted Rand Index (ARI): Measures the similarity between the predicted clustering and the ground truth cell types.
- Normalized Mutual Information (NMI): Evaluates the mutual dependence between predicted and true labels.

## 4.3 Main Clustering Results

We evaluate the clustering performance of CCCVAE and three baseline models-Vanilla VAE, GMVAE, and scVI-across four diverse single-cell datasets: PBMC4K, Opium, Pancreas, and PBMC12K. Clustering quality is assessed using two standard metrics: Adjusted Rand Index (ARI) and Normalized Mutual Information (NMI). The results are summarized in Table 1.

CCCVAE consistently achieves the highest ARI and NMI scores across all datasets. These gains are particularly evident on Pancreas and PBMC12K, which are more biologically complex and present greater challenges for cell-type separation. For example, on the Pancreas dataset:

- ARI improves from 0.177 (Vanilla VAE) and 0.227 (scVI) to 0.287 (CCCVAE),
- NMI improves from 0.295 (Vanilla VAE) and 0.436 (scVI) to 0.480 (CCCVAE).

Similarly, on the PBMC12K dataset:

- CCCVAE reaches an ARI of **0.462**, surpassing scVI's 0.460 and significantly outperforming GMVAE (0.222),

- CCCVAE attains the highest NMI of 0.670, exceeding scVI's 0.646 and Vanilla VAE's 0.567.

These improvements highlight CCCVAE's ability to model cell-type-specific structures with higher biological fidelity.

To further support these quantitative results, we present UMAP visualizations of the latent space for the Pancreas dataset (Figure 3). Compared to scVI, which shows more diffuse and overlapping clusters, CCCVAE produces well-separated and compact clusters that align closely with known cell types. This reflects its improved representation of the intrinsic biological structure.

We attribute CCCVAE's superior clustering performance to its novel integration of Cell-Cell Communication (CCC) priors through a sparse Gaussian Process layer. These priors encode biologically informed interactions-such as ligand-receptor signaling-into the latent space. As a result, CCCVAE captures not only individual expression patterns but also relational dependencies that guide cell differentiation and spatial organization. This biologically grounded structure encourages the emergence of more coherent, interaction-aware clusters, setting CCCVAE apart from existing unsupervised models.

**Table 1:** Clustering Results of Vanilla VAE, GMVAE, scVI, and CCCVAE on Four Datasets

Model	PBMC4K ARI	PBMC4K NMI	Opium ARI	Opium NMI	Pancreas ARI	Pancreas NMI	PBMC12K ARI	PBMC12K NMI
Vanilla VAE	0.402	0.259	0.119	0.332	0.177	0.295	0.342	0.567
GMVAE	0.015	0.121	0.179	0.214	0.028	0.152	0.222	0.218
scVI	0.403	<b>0.610</b>	0.387	0.670	0.227	0.436	0.460	0.646
CCCVAE	<b>0.450</b>	0.605	<b>0.418</b>	<b>0.703</b>	<b>0.287</b>	<b>0.480</b>	<b>0.462</b>	<b>0.670</b>

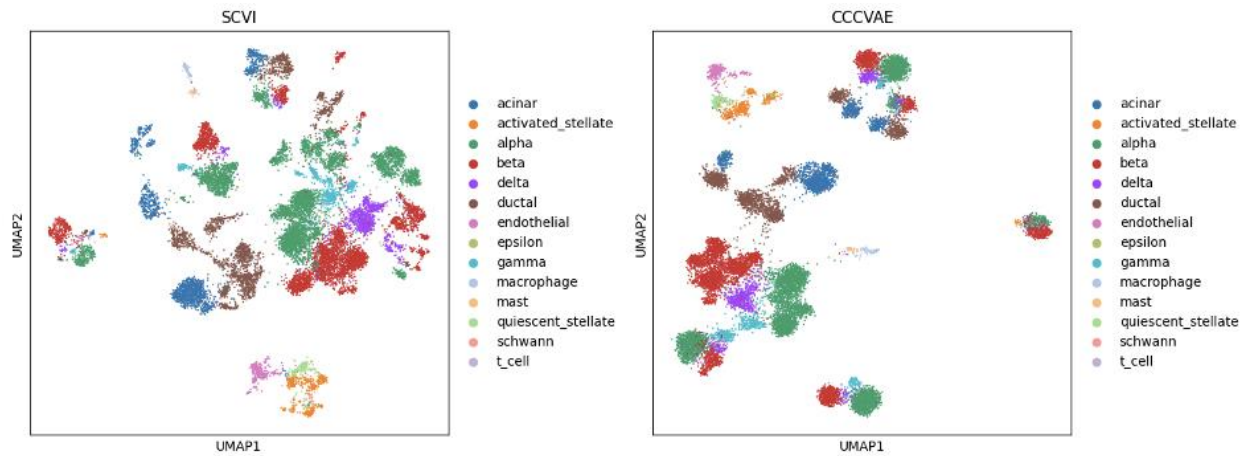


**Figure 3:** The visualization of the clustering result on Opium dataset.

#### 4.4 CCC Improvement Analysis

To specifically evaluate the extent to which models preserve Cell-Cell Communication (CCC) structure in the latent space, we conduct a CCC-based evaluation using the PBMC4K and Pancreas datasets. We first use scVI and our proposed CCCVAE to generate latent representations of all cells and apply K-means clustering to assign cluster labels. Next, we compute group-level communication matrices via the CellChat framework, resulting in an adjacency matrix of size  $n\_cluster \times n\_cluster$ , where each entry reflects the communication strength between two cell clusters.

To interpret the preserved signaling structure, we analyze and visualize the resulting communication matrices by plotting the distribution of edge weights, shown as both histograms and cumulative distribution functions (CDFs) in Figure 4. Each subplot compares the edge weight distributions obtained from CCCVAE (blue) and scVI (orange).

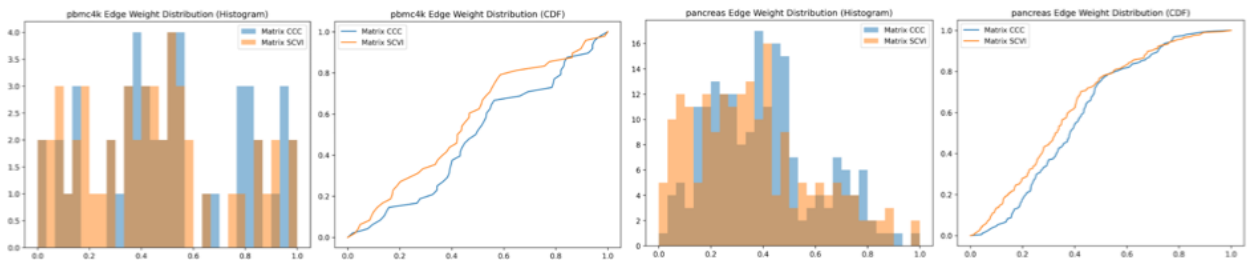


**Figure 4:** Comparison of edge weight distributions from cell-cell communication graphs derived using latent representations from scVI and CCCVAE on the PBMC4K and Pancreas datasets. Histograms (left) and CDFs (right) show that CCCVAE produces more variable and stronger edge weights, indicating enhanced preservation of inter-cluster signaling structure in the latent space.

Across both datasets, several key trends emerge:

#### Higher Edge Weight Variability:

CCCVAE yields a broader spread of edge weights, as seen in the histograms, suggesting that it better differentiates between strong and weak inter-cluster communications. In contrast, the distributions from scVI are more concentrated around mid-range values, indicating a lack of contrast in inferred communication strengths.

#### Right-Shifted CDFs:

The CDF curves for CCCVAE are consistently right-shifted compared to those from scVI, meaning a larger proportion of edges have higher weights. This shift indicates that CCCVAE captures more intense signaling relationships between cell groups.

#### Dataset Consistency:

These trends hold across both PBMC4K and Pancreas datasets, showcasing the robustness of CCCVAE in different biological contexts. Notably, for the pancreas dataset, the histogram shows

a clear enhancement in edge frequency across medium-to-high weight ranges, reinforcing the model's ability to recover biologically plausible signaling pathways.

These findings support our hypothesis that explicitly modeling cell-cell communication during training promotes the emergence of functionally coherent latent structures. By embedding communication priors into the generative process, CCCVAE encourages the latent space to reflect not just transcriptomic similarity, but also functional interaction patterns. This leads to improved interpretability and utility in downstream tasks such as pathway analysis, cell type interaction mapping, and therapeutic target discovery.

#### **4.5 Ablation Study**

To assess the contribution of individual model components, we conducted ablation studies on two critical hyperparameters: the number of Gaussian Process (GP) latent dimensions and the KL-divergence regularization weight  $\beta$ . These analyses help identify optimal configurations that balance expressive power and generalization.

##### **Gaussian Process Dimension**

We investigated the impact of varying the number of latent dimensions assigned to the GP module while keeping the total latent dimension fixed at 80 . Specifically, we evaluated configurations where 4, 8, 16, or 32 dimensions were assigned to the GP, with the remaining dimensions modeled as standard Gaussian.

As shown in Figure 5, ARI scores across all four datasets (PBMC4K, Opium, Pancreas, and PBMC12K) exhibit a consistent trend. Performance steadily improves from 4 to 16 GP dimensions, peaking at 16. However, when increasing to 32 dimensions, performance declines. This suggests that allocating too few dimensions underutilizes the GP's modeling capacity for cell-cell communication, while too many may lead to overfitting or loss of general latent structure. The 16-dimensional GP setting strikes a balance between expressiveness and regularization.

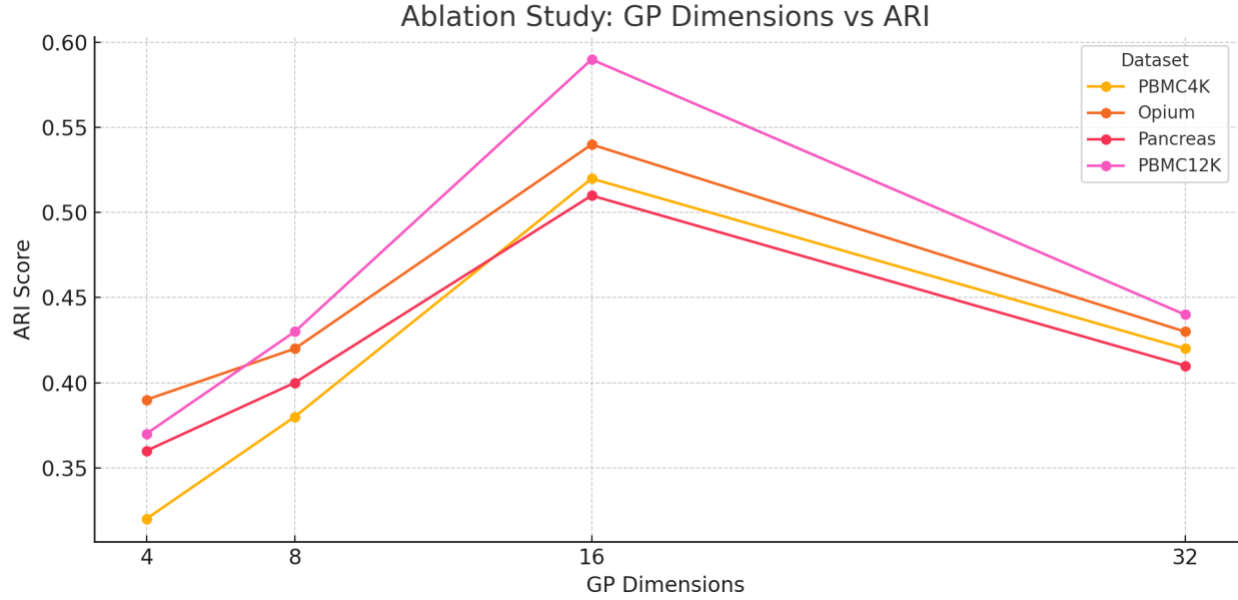


**Figure 5:** Ablation Study of GP Dimensions (ARI as metric)

### KL-Divergence Weight $\beta$

We next evaluated the influence of the KL-divergence coefficient  $\beta$ , which controls the strength of latent space regularization in the VAE objective. We tested values [0.01,0.02,0.05,0.1,0.2], observing their effect on clustering quality via ARI scores.

As shown in Figure 6, low  $\beta$  values (0.01 and 0.02) consistently yielded higher ARI scores. This indicates that allowing more flexibility in the latent space (i.e., weaker prior matching) helps retain complex biological variation useful for clustering. Higher  $\beta$  values, on the other hand, result in excessive regularization that impairs clustering by collapsing the latent space. These findings emphasize the importance of tuning  $\beta$  to avoid underfitting or over-regularization.

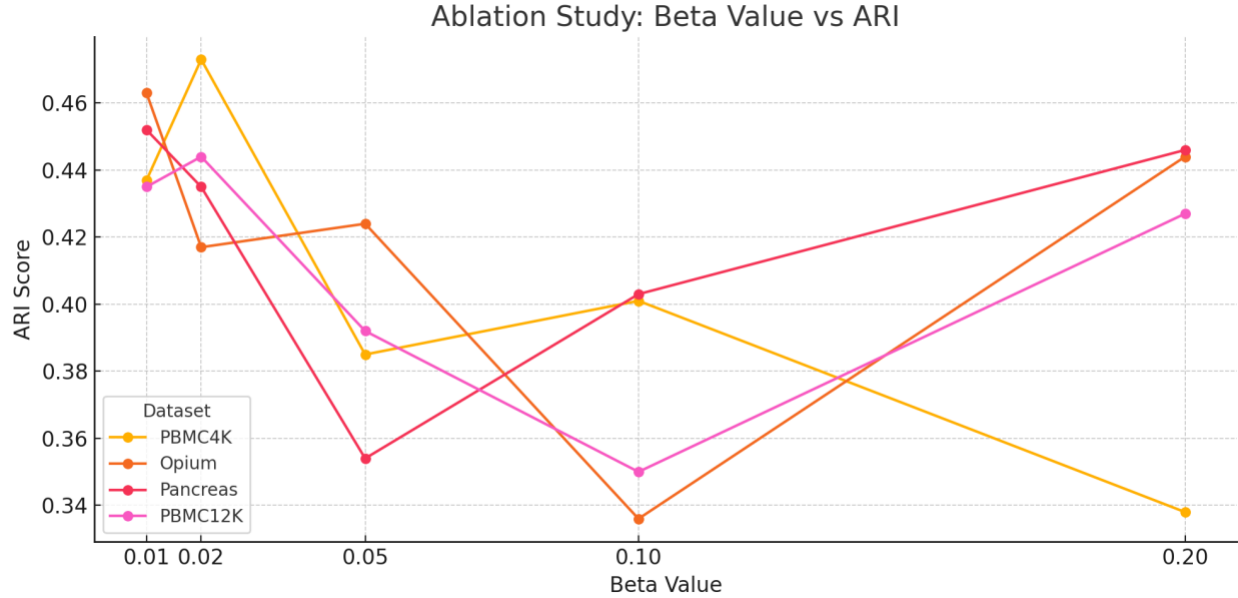


**Figure 6:** Ablation Study of Beta Value (ARI as metric)

## 5. Conclusion

In this work, we proposed CCCVAE, a novel variational framework that integrates cell-cell communication signals into the latent representation learning of single-cell data. By leveraging a Sparse Gaussian Process with a biologically informed CCC kernel, our model captures intercellular relationships that are overlooked in conventional approaches. Through comprehensive experiments across multiple datasets, CCCVAE demonstrates consistent improvements in clustering performance, outperforming baseline methods such as Vanilla VAE, GMVAE, and scVI. Ablation studies further highlight the critical role of the CCC prior and design choices in enhancing latent structure. Overall, CCCVAE offers a principled and effective solution to incorporate biological prior knowledge into deep generative models, paving the way for more accurate and interpretable single-cell analyses. Future directions include extending CCCVAE to multi-omics data and exploring its potential in dynamic cell communication modeling.

## References

- [1] Kingma, Diederik P., and Max Welling. 'Auto-encoding variational Bayes.' arXiv preprint arXiv:1312.6114 (2013).
- [2] Lopez, Romain, et al. 'Deep generative modeling for single-cell transcriptomics.' Nature Methods 15.12 (2018): 1053-1058.
- [3] Grønbech, Casper F., et al. 'scVAE: Variational auto-encoders for single-cell gene expression data.' Bioinformatics 36.16 (2020): 4415-4422.

- [4] Gayoso, Adam, et al. 'A Python library for probabilistic analysis of single-cell omics data.' *Nature Biotechnology* 40.2 (2022): 163-166.
- [5] Lotfollahi, Mohammad, et al. 'scGen predicts single-cell perturbation responses.' *Nature Methods* 16.8 (2019): 715-721.
- [6] Eraslan, Gökcen, et al. 'Single-cell RNA-seq denoising using a deep count autoencoder.' *Nature Communications* 10.1 (2019): 390.
- [7] Jin, Shuxiong, et al. 'Inference and analysis of cell-cell communication using CellChat.' *Nature Communications* 12.1 (2021): 1088.
- [8] Browaeys, Robin, Wouter Saelens, and Yvan Saeys. 'NicheNet: modeling intercellular communication by linking ligands to target genes.' *Nature Methods* 17.2 (2020): 159-162.
- [9] Efremova, Mirjana, et al. 'CellPhoneDB: inferring cell–cell communication from combined expression of multi-subunit ligand–receptor complexes.' *Nature Protocols* 15.4 (2020): 1484-1506.
- [10] Ramilowski, Jonas A., et al. 'A draft network of ligand–receptor-mediated multicellular signalling in human.' *Nature Communications* 6.1 (2015): 7866.
- [11] Armingol, Enrique, et al. 'Deciphering cell–cell interactions and communication from gene expression.' *Nature Reviews Genetics* 22.2 (2021): 71-88.
- [12] Giladi, Amir, and Ido Amit. 'Immunology: Single-cell genomics reveals immune cell signaling.' *Nature* 561.7724 (2018): 455-456.
- [13] Tirosh, Itay, et al. 'Dissecting the multicellular ecosystem of metastatic melanoma by single-cell RNA-seq.' *Science* 352.6282 (2016): 189-196.
- [14] Plasschaert, Laura WL, et al. 'A single-cell atlas of the airway epithelium reveals the CFTR-rich pulmonary ionocyte.' *Nature* 560.7718 (2018): 377-381.
- [15] Svensson, Valentine, Roshan Sharma, and Lior Pachter. 'Scaling up spatial transcriptomics for tissue-wide gene expression mapping.' *Nature Biotechnology* 38.6 (2020): 629-630.
- [16] Dong, Zepeng, and Guo-Cheng Yuan. 'SpatialDWLS: accurate deconvolution of spatial transcriptomic data.' *Genome Biology* 21.1 (2020): 1-10.
- [17] Wu, Ke, et al. 'Contrastive scRNA-seq representation learning for unsupervised cell type clustering and annotation.' *bioRxiv* (2021).
- [18] Ashuach, Tal, et al. 'PeakVI: A deep generative model for single-cell chromatin accessibility analysis.' *Cell Reports Methods* 1.6 (2021): 100105.
- [19] Titsias, Michalis K. 'Variational learning of inducing variables in sparse Gaussian processes.' *Artificial Intelligence and Statistics*. PMLR, 2009.



- [20] Hensman, James, Nicolo Fusi, and Neil D. Lawrence. 'Gaussian processes for big data.' arXiv preprint arXiv:1309.6835 (2013).
- [21] Heinonen, Markus, et al. 'Non-stationary Gaussian process regression with Hamiltonian Monte Carlo.' Artificial Intelligence and Statistics. PMLR, 2016.
- [22] Abu-Mostafa, Yaser S., Malik Magdon-Ismail, and Hsuan-Tien Lin. 'Learning from data.' Vol. 4. New York: AMLBook, 2012.
- [23] Rahimi, Ali, and Benjamin Recht. 'Random features for large-scale kernel machines.' Advances in Neural Information Processing Systems 20 (2008).
- [24] Rasmussen, Carl Edward, and Christopher K. I. Williams. 'Gaussian processes for machine learning.' MIT Press, 2006.
- [25] Wilson, Andrew Gordon, and Ryan Prescott Adams. 'Gaussian process kernels for pattern discovery and extrapolation.' International Conference on Machine Learning. PMLR, 2013.
- [26] Zheng, Guo-Cheng, et al. 'Massively parallel digital transcriptional profiling of single cells.' Nature Communications 8.1 (2017): 14049.
- [27] Tabula Muris Consortium. 'Single-cell transcriptomics of 20 mouse organs creates a Tabula Muris.' Nature 562.7727 (2018): 367-372.
- [28] Butler, Andrew, et al. 'Integrating single-cell transcriptomic data across different conditions, technologies, and species.' Nature Biotechnology 36.5 (2018): 411-420.
- [29] Luecken, Malte D., and Fabian J. Theis. 'Current best practices in single-cell RNA-seq analysis: a tutorial.' Molecular Systems Biology 15.6 (2019): e8746.
- [30] Vinh, Nguyen Xuan, Julien Epps, and James Bailey. 'Information theoretic measures for clusterings comparison: Variants, properties, normalization and correction for chance.' Journal of Machine Learning Research 11.Oct (2010): 2837-2854.
- [31] McInnes, Leland, John Healy, and James Melville. 'UMAP: Uniform manifold approximation and projection for dimension reduction.' arXiv preprint arXiv:1802.03426 (2018).
- [32] Bengio, Yoshua, Aaron Courville, and Pascal Vincent. 'Representation learning: A review and new perspectives.' IEEE Transactions on Pattern Analysis and Machine Intelligence 35.8 (2013): 1798-1828.
- [33] Higgins, Irina, et al. 'beta-VAE: Learning basic visual concepts with a constrained variational framework.' ICLR (2017).
- [34] Alemi, Alexander A., et al. 'Deep variational information bottleneck.' ICLR (2017).

## Appendix :

### A. Positive-Definiteness of the Kernel

The final kernel  $K_{CCC}$  remains positive-definite because:

- The Cauchy kernel  $K_{\text{Cauchy}}$  is positive-definite by design, as it represents a valid covariance function for a Gaussian Process.
- The propagation matrix  $P$  is constructed using the communication matrix, which is symmetric and scaled by the identity matrix. As  $P$  is derived from the communication matrix, which is positive semidefinite, and it is modified by adding the identity matrix, it remains positive semi-definite.
- The product of two positive-definite matrices (i.e.,  $K_{\text{Cauchy}}$  and  $P$ ) preserves positive-definiteness, ensuring the overall kernel is valid for Gaussian Process inference.

Thus, this kernel construction ensures both biological relevance (cell communication is captured) and computational validity (positive-definiteness for inference).

### *Proof*

To formally prove that  $K_{CCC} = K_{\text{Cauchy}} \cdot P \cdot K_{\text{Cauchy}}^T$  is positive definite, given that  $K_{\text{Cauchy}}$  and  $P$  are positive definite, we need to show that for any non-zero vector  $v$ , the quadratic form  $v^T K_{CCC} v$  is strictly positive.

1. Define the quadratic form for  $K_{CCC}$  :

We start with the quadratic form  $v^T K_{CCC} v$ , where  $K_{CCC} = K_{\text{Cauchy}} \cdot P \cdot K_{\text{Cauchy}}^T$ .

$$v^T K_{CCC} v = v^T (K_{\text{Cauchy}} \cdot P \cdot K_{\text{Cauchy}}^T) v$$

2. Rearrange the expression:

We can rewrite the quadratic form by associating the matrices:

$$v^T K_{CCC} v = (K_{\text{Cauchy}}^T v)^T P (K_{\text{Cauchy}} v)$$

This is equivalent to:

$$v^T K_{CCC} v = z^T P z$$

where  $z = K_{\text{Cauchy}}^T v$ .

### 3. Positive Definiteness of $P$ :

Since  $P$  is positive definite, we know that for any non-zero vector  $z$ ,  $z^T P z > 0$ . This follows directly from the definition of a positive definite matrix.

### 4. Non-zero vector $z$ :

The vector  $z = K_{\text{Cauchy}}^T v$  is non-zero for any non-zero  $v$ , because  $K_{\text{Cauchy}}$  is assumed to be positive definite. A positive definite matrix does not map non-zero vectors to the zero vector, so  $z \neq 0$  for  $v \neq 0$ .

### 5. Conclusion:

Since  $P$  is positive definite, for any non-zero vector  $z$ , we have:

$$z^T P z > 0$$

Therefore, the quadratic form  $v^T K_{\text{CCC}} v$  is strictly positive for any non-zero vector  $v$ , which implies that  $K_{\text{CCC}}$  is positive definite.

## B. Sparse GP Prior Correctness

We provide the detailed derivation showing that our sparse variational Gaussian Process (GP) prior correctly approximates the posterior over the CCC-aware latent dimensions  $z_i^{(1)}$ .

### B.1 Model Assumptions

For each CCC-aware latent dimension  $l \in \{1, \dots, \ell\}$  :

- $f_l(x) \sim \mathcal{GP}(0, K_{\text{CCC}}(x, x'))$  (Zero-mean GP with CCC kernel.)
- Inducing points  $Z_u = [u_1, \dots, u_m] \in \mathbb{R}^{m \times G}$  with outputs  $u_l \in \mathbb{R}^m$ .
- Given observed noisy data  $(x_i, y_i)$ , we assume:

$$y_i = f_l(x_i) + \epsilon_i, \epsilon_i \sim \mathcal{N}(0, \sigma_i^2)$$

where  $\sigma_i^2$  is the encoder-predicted noise variance.

- Variational distribution over inducing outputs:

$$q(u_l) = \mathcal{N}(\mu_l, A_l)$$

### B.2 Variational Approximation of Posterior

Given the standard variational GP framework (Titsias, 2009), the exact posterior is intractable. We introduce  $q(u_l)$  and derive an approximate posterior  $q(f_l(x))$  as follows:

The joint prior over  $f_l(X)$  and  $u_l$  is:

$$p(f_l(X), u_l) = \mathcal{N}\left(0, \begin{bmatrix} K_{nn} & K_{nm} \\ K_{mn} & K_{mm} \end{bmatrix}\right)$$

where:

- $K_{nn}$  is the kernel between training points.
- $K_{nm}, K_{mn}$  are cross-covariances.
- $K_{mm}$  is the kernel among inducing points.

Using conditional properties of Gaussian distributions:

$$p(f_l(X) | u_l) = \mathcal{N}(K_{nm}K_{mm}^{-1}u_l, K_{nn} - K_{nm}K_{mm}^{-1}K_{mn})$$

Thus, the variational posterior becomes:

$$q(f_l(X)) = \int p(f_l(X) | u_l)q(u_l)du_l$$

Since  $p(f_l(X) | u_l)$  and  $q(u_l)$  are both Gaussian,  $q(f_l(X))$  remains Gaussian, and its mean and covariance are:

$$\begin{aligned} \mathbb{E}_{q(u_l)}[f_l(x)] &= K_{nm}K_{mm}^{-1}\mu_l \\ \text{Cov}_{q(u_l)}[f_l(x)] &= K_{nn} - K_{nm}K_{mm}^{-1}K_{mn} + K_{nm}K_{mm}^{-1}A_lK_{mm}^{-1}K_{mn} \end{aligned}$$

### B.3 Minibatch Correction

Since we optimize using minibatches, following (Hensman et al., 2013), we rescale the noise by  $\frac{N}{b}$ :

- Scaled noise variance:  $\tilde{\sigma}_i^2 = \frac{b}{N}\sigma_i^2$ .

The corrected variational posterior for minibatch inference is:

$$q(f_l(x_i)) = \mathcal{N}(\mu_l(x_i), \sigma_l^2(x_i))$$

with:

$$\mu_l(x_i) = \frac{N}{b} K_{x_i m} \left( K_{mm} + \frac{N}{b} K_{mn} \text{diag}(\sigma^{-2}) K_{nm} \right)^{-1} K_{mn} \text{diag}(\sigma^{-2}) y$$

$$\sigma_l^2(x_i) = K_{x_i x_i} - K_{x_i m} K_{mm}^{-1} K_{m x_i} + K_{x_i m} \left( K_{mm} + \frac{N}{b} K_{mn} \text{diag}(\sigma^{-2}) K_{nm} \right)^{-1} K_{m x_i}$$

These are exactly the formulas implemented in our method.

#### B.4 Variational Evidence Lower Bound (ELBO)

The sparse GP ELBO for each CCC-aware dimension  $l$  is:

$$\mathcal{L}_{\text{GP}}^{(l)} = \mathbb{E}_{q(f_l(x))} [\log p(y \mid f_l(x))] - \text{KL}(q(u_l) \parallel p(u_l))$$

Explicitly:

- The likelihood term includes corrections for the minibatch noise.
- The KL divergence is:

$$\text{KL}(q(u_l) \parallel p(u_l)) = \frac{1}{2} \left( \log \frac{\det K_{mm}}{\det A_i} - m + \text{Tr}(K_{mm}^{-1} A_i) + \mu_i^\top K_{mm}^{-1} \mu_i \right)$$

Thus, the variational lower bound is minimized correctly through minibatch-optimized ELBO.